Structural properties and electronic structure of HfO_2-ZrO_2 composite films

Deok-Yong Cho,[1,*] Hyung-Suk Jung,[2] and Cheol Seong Hwang[2,†]
[1]*CSCMR & FPRD, Department of Physics and Astronomy, Seoul National University, Seoul 151-747, Korea*
[2]*WCU Hybrid Materials Program, Department of Materials Science and Engineering, and Inter-University Semiconductor Research Center, Seoul National University, Seoul 151-744, Korea*
(Received 14 June 2010; published 13 September 2010)

This study examined the structural evolution of ultrathin $Hf_{1-x}Zr_xO_2$ composite films with various mixing ratios (x=0,0.1,0.3,0.5,0.7,0.9,1) prepared by atomic layer deposition using x-ray photoelectron spectroscopy (XPS), x-ray absorption spectroscopy (XAS), and x-ray absorption fine structure (XAFS) analysis. As the relative Zr concentration (x) was increased, the composite films underwent a martensitic transition from monoclinic to tetragonal crystal structures near x=0.5–0.7. Zr K- and Hf L_3-edge XAFS revealed a change in the local structures near the Zr and Hf atoms with changes in the crystal structure. At a low Zr content ($x \leq 0.5$), the next-nearest-neighbor coordination in the monoclinic (m) local structure showed significant structural disorder due to diverse structural reconstruction from the tetragonal (t) local structure. Combined XPS and O K-edge XAS studies revealed a decrease in the conduction-band (CB) edge energy with increasing x, whereas the valence-band edge energies were invariant. The evolution in the CB structures was analyzed using the concept of metal-ion crystal fields in the t and m cluster models.

DOI: 10.1103/PhysRevB.82.094104 PACS number(s): 77.55.D−, 61.05.cj, 78.70.Dm

I. INTRODUCTION

As the dimension of complementary metal-oxide semiconductor field-effect transistor (CMOSFET) shrinks, the downscaling of the SiO_2 gate dielectric reaches its physical limit due to the high leakage current and reliability problems. Hf-based gate dielectrics are considered one of the most promising candidates for replacing SiO_2 gate dielectrics. Hf-based gate insulators with a metal gate have already been implemented in mass production.[1] However, some challenging problems still remain, such as high threshold voltage (V_{th}), large amounts of oxide trap charges, and other reliability concerns.[2–7] The addition of other atoms, such as N, Si, Al, or Zr, has been reported to overcome those problems in Hf-based gate oxides.[3,8,9] Recently, a mixture of HfO_2 and ZrO_2, i.e., HfZrO, has attracted increasing attention as a gate dielectric in CMOSFET (Refs. 10–12) because it guarantees significantly improved electrical performance and bias temperature instability (BTI) characteristics compared to HfO_2.[9]

The improved CMOSFET characteristics in the case of the HfZrO gate dielectrics are due to the superior physical properties of HfZrO than HfO_2.[9] Aside from the interface effect, in which various atomic configurations at the Si interface affect the electrical properties of the CMOSFETs,[13–15] the bulk properties, such as the defect formation energy, grain size, or atomic coordination in the gate dielectrics, can induce a range of electrochemical properties in the oxides. The bulk defect states in the high-k oxide undoubtedly degrade the dielectric properties even reducing the band gap.[16–18] The smaller grain size and enhanced uniformity in the HfZrO compared to those in HfO_2 improve the V_{th} and BTI characteristics indirectly by controlling the trap states.[9] The atomic coordination in the Hf-O and Zr-O bonds should also be an important factor, as shown in Hf or Zr silicates.[19,20] In the case of HfO_2, the most stable crystal structure is a monoclinic ($m;P2_1/c$) phase, so the local Hf-O clusters prefer to have sevenfold coordination at room temperature.[21,22] In contrast, ZrO_2 favors a tetragonal crystal structure ($t;P4_2/nmc$) if the film is as thin, as in actual gate dielectrics (approximately few nanometers). Hence, the Zr-O bonds prefer to form eightfold coordination at room temperature.[20,23,24] Therefore, the mixing of HfO_2 and ZrO_2 should induce a nontrivial local phase transformation as the composition ratio (x) changes. In addition, the local dielectric polarization is determined mainly from the local structures, except for minor contributions from charge transfer between clusters.[20,25] Therefore, it is important to examine the evolution of local structures with increasing x in $Hf_{1-x}Zr_xO_2$ composite films.

II. EXPERIMENTAL METHODS

80-Å-thick $Hf_{1-x}Zr_xO_2$ composite films with various mixing ratios (x=0,0.1,0.3,0.5,0.7,0.9,1) were deposited on HF-cleaned Si wafers by plasma-enhanced atomic-layer deposition (PEALD). $Hf[N(C_2H_5)(CH_3)]_4$, $Zr[N(C_2H_5)(CH_3)]_4$, and plasma-activated O_2 were used as the Hf precursor, Zr precursor, and oxidant, respectively. The wafer temperature was 280 °C. After the PEALD cycles, rapid thermal annealing was performed in an N_2 ambiance to improve the crystallinity. Although the films crystallized at 500–550 °C, the annealing was performed at 950 °C to ensure the crystallization. The high-temperature treatment did not influence the chemistry or structure of the films. X-ray fluorescence confirmed that the composition ratios (x) in the films were similar to those deduced from the respective PEALD cycles of the Hf and Zr sourcing processes.

The local structures near the Hf and Zr atoms in the $Hf_{1-x}Zr_xO_2$ films were examined by x-ray absorption fine structure (XAFS) analysis. Fourier transformations of the extended XAFS (EXAFS) oscillations in the Hf L_3- and Zr K-edge x-ray absorption spectroscopy (XAS) spectra provide real space information on the coordination of the respective atoms. The experiment was carried out at room tem-

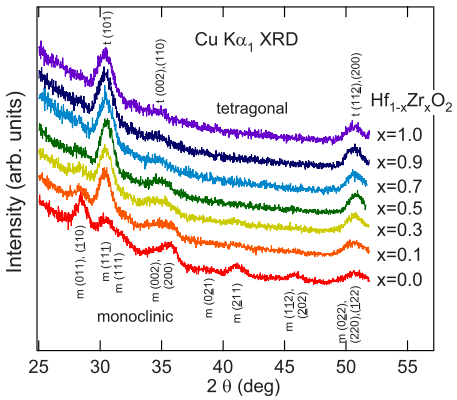

FIG. 1. (Color online) θ-2θ XRD patterns of the $Hf_{1-x}Zr_xO_2$ composite films with the peak assignments according to the $P2_1/c$ and $P4_2/nmc$ symmetries for the m and t phases, respectively.

perature at the 3C1 beamline in Pohang Light Source (PLS). The conduction-band (CB) structure was also examined using O K-edge XAS. Although O K-edge XAS primarily reflects the unoccupied O $2p$ states, it is frequently used to examine the metal-ion CB, which is well hybridized with the O $2p$ wave functions. The O K-edge XAS was performed at room temperature at the 2A beamline in the PLS. X-ray photoelectron spectroscopy (XPS) was performed using a monochromatic Al $K\alpha$ source. The crystal structures of the composite films were examined by x-ray diffraction (XRD) using a monochromatic Cu $K\alpha_1$ source.

III. RESULTS AND DISCUSSION

A. X-ray diffraction

Figure 1 shows the θ-2θ XRD patterns of the $Hf_{1-x}Zr_xO_2$ films. The peaks were assigned according to the notations of the $P2_1/c$ and $P4_2/nmc$ symmetries for the m and t phases, respectively. Although the overall features are broad due to the low film thickness, the features clearly show a change in the crystal structure from m to t with increasing x. It appears that the m phase survived up to $x=0.5$, showing the m (011), $(\bar{1}10)$ peaks, but the difference in the m (011) to m $(11\bar{1})$ [or $t(101)$] intensity ratio between $x=0.3$ and $x=0.0$, indicates that their crystal structures are not the same as each other. In Fig. 1, it is unclear if the discrepancy originates from the inhomogeneity of the sample or truly different structure factors. The former case, i.e., inhomogeneity, refers to a case when the composite film has more than one structural domain hence the crystal structure of one domain is monoclinic and that of another domain is tetragonal resulting in the coexistence of both diffraction features. The latter case refers to when the films are uniform and slight local coordination changes modulate the intensity ratio of the XRD pattern. The XAFS analyses (Figs. 2 and 3) in the next section will clear this vagueness showing that our $Hf_{1-x}Zr_xO_2$ system fell on the latter case.

B. X-ray absorption fine structures

XAFS in the XAS spectrum reflects the probability that photoexcited electrons might be backscattered by adjacent

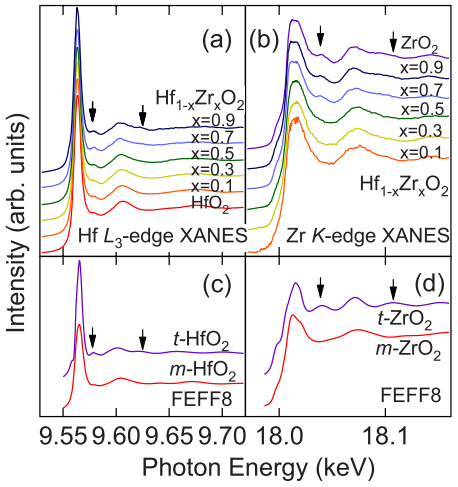

FIG. 2. (Color online) Normalized XANES of the $Hf_{1-x}Zr_xO_2$ films taken at (a) Hf L_3 edge and (b) Zr K edge. Results of full multiple-scattering XANES simulation implemented by FEFF8 for theoretical t-Hf[Zr]O_2 or m-Hf[Zr]O_2, were appended in (c) [(d)]. The prominences of the features for $x \geq 0.7$, highlighted by the arrows, indicate the tetragonal local structure near both Hf and Zr atoms.

atoms and reabsorbed in the photon-absorbing atom. For given atomic species of photon absorber and scatterers, the electron-atom scattering profile is determined mainly by the kinetic energy of the quasifree electrons.[26] If the kinetic energy of the final-state electron is high enough (typically >30 eV) or the photon energy is far above the edge energy, the reabsorbed electrons are dominated by direct backscattering only, so that EXAFS, which frequently employs the high kinetic-energy range, reflects the direct bonding information, such as the bond length and its variance due to thermal or

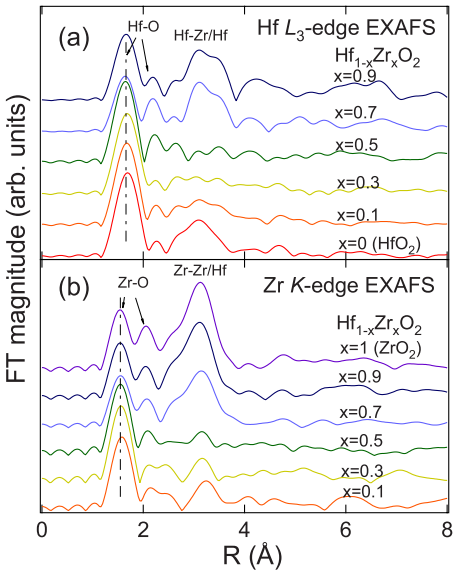

FIG. 3. (Color online) Fourier-transformed EXAFS magnitudes of the $Hf_{1-x}Zr_xO_2$ films taken at (a) Hf L_3 edge and (b) Zr K edge. Splits of Hf(Zr)-O bond length for $x \geq 0.7$ evidences the tetragonal local structures. Features of Hf(Zr)-Hf/Zr for $x \leq 0.5$ were suppressed due to the significantly enhanced structural disorder.

TABLE I. The local structures of the $Hf_{1-x}Zr_xO_2$ near Hf and Zr atoms deduced from the XAFS analyses. The *m* and *t* denote the monoclinic and tetragonal *local* structures, respectively.

	x						
Atoms	0 (HfO_2)	0.1	0.3	0.5	0.7	0.9	1 (ZrO_2)
Hf	*m*	*m*	*m*	*m*	*t*	*t*	
Zr		*m*	*m*	*m*	*t*	*t*	*t*

structural disorder. On the other hand, if the electron kinetic energy is low (typically <40 eV) or the photon energy is near the edge energy, multiple-scattering events near the photon absorber make a contribution to the x-ray absorption near-edge structure (XANES). Therefore, XANES reflects the details in the symmetry of the local coordination but is less sensitive to the bonding information than EXAFS. Hence, XANES was used to determine the local coordination whereas the EXAFS were used to deduce the bonding information for the $Hf_{1-x}Zr_xO_2$ films.

1. XANES

Figure 2 shows the XANES in the XAS spectra of the $Hf_{1-x}Zr_xO_2$ films taken near the (a) Hf L_3 edge ($h\nu \sim 9.56$ keV) and (b) Zr *K* edge ($h\nu \sim 18.01$ keV). The highest peaks at $h\nu \sim 9.56$ keV in Fig. 2(a) reflect the Hf $2p_{3/2} \rightarrow 5d$ transition and features above $h\nu \sim 9.57$ keV are due to the transition to the $6sd$ continuum. The features in Fig. 2(b) reflect the Zr $1s \rightarrow 5p$ continuum transition. These features became more prominent as the Zr content (*x*) was increased, as highlighted by the arrows in both figures. To determine the origin of the features, XANES simulations were performed at both edges using *ab initio* full multiple-scattering code, FEFF8.[27] The simulations were performed for *t*-HfO_2 and *m*-HfO_2 and ZrO_2 with the structure information taken from the literature.[22,28,29] Here the muffin-tin potentials for electron-atom scattering were calculated self-consistently and all multiple scatterings within a radius of 6 Å (with origin at the photon absorber) up to infinite-scattering order were considered. The effects of the limited inelastic mean-free paths of the final state electrons or thermal disorder were excluded.

Figures 2(c) and 2(d) show the results of the simulations for the four configurations: *m*-HfO_2, *t*-HfO_2, *m*-ZrO_2, and *t*-ZrO_2. The protrusion of the features for the case of *t*-HfO_2 and *t*-ZrO_2 was clearly observed, as shown by the arrows in the respective figures. The correspondence in the overall line shapes to the experimental spectra indicates that the change in the XANES in Figs. 2(a) and 2(b) is associated with a change in the local structures. At $x \leq 0.5$, the local structures of the Hf and Zr atoms were similar to those in the monoclinic HfO_2 or ZrO_2: sevenfold Hf(Zr)-O coordination. For $x \geq 0.7$, the local structures were similar to those in the tetragonal HfO_2 or ZrO_2: eightfold Hf(Zr)-O coordination. Table I summarizes the local structures of the $Hf_{1-x}ZrO_2$ near the Hf and Zr atoms, as deduced from XANES analyses. This tendency is consistent with the results of EXAFS analyses shown in Fig. 3.

The local structures of the Hf and Zr atoms changed abruptly between $x=0.5-0.7$. This abruptness suggests that the *m*-*t* transition occurs martensitically[30] throughout the films. Otherwise, the transition should have occurred gradually with increasing Zr content if the apparent *m*-*t* transition was caused by the prevailing nucleated structural domains without an interaction between the domains, as suggested by the effective-medium theory in noninteracting grains.[31,32] Therefore, the abruptness itself suggests that the structural change in these films is relevant to the atomic scale stabilization in the networks of the Hf(Zr)-O clusters.

The system, $x=1/2$ ($HfZrO_4$), has a monoclinic local structure. This asymmetry with respect to *x*, reflects the stability of the monoclinic structure in low Zr contents HfZrO. The total energy of the mixed oxide films can be represented approximately by the sum of the energy with each cluster. Since the Zr-O clusters prefer tetragonal coordination, whereas the Hf-O clusters favor monoclinic coordination, it can be understood that the energy gain caused by monoclinic Hf-O coordination is larger than the energy loss caused by losing tetragonal Zr-O coordination in the $(HfO_2)_{0.5}$-$(ZrO_2)_{0.5}$.

2. EXAFS

Figure 3 shows the Fourier-transformed (FT) magnitudes of the (a) Hf L_3-edge and (b) Zr *K*-edge EXAFS for the $Hf_{1-x}Zr_xO_2$ films. The abrupt changes in the overall line shapes with increasing *x*, were also observed for both edges, consistently with the results of XANES (in Fig. 2). According to the half-path length *R*, the features at $R \sim 1.7$ Å and $R \sim 3$ Å were assigned to Hf(Zr)-O and Hf(Zr)-Zr/Hf bonds, respectively.[33–35] The bond length of Hf(Zr)-O splits into two at $x \geq 0.7$ with the tetragonal local structures. To obtain the detailed information on the bonds, the FT EXAFS spectra were fitted considering the single scatterings only. Table II presents the fitting results for the $x=0.3$ and $x=0.7$ samples; the phase-corrected interatomic distances ($R+\Delta$) and Debye-Waller factors (σ^2) of the Hf(Zr)-O and Hf(Zr)-Hf/Zr bonds were obtained. The local structures of the $x=0.3$ and $x=0.7$ samples were assumed to be monoclinic and tetragonal, respectively, in accordance with the XANES finding. The Hf(Zr) atoms have seven O and 11 Hf/Zr neighboring atoms in the monoclinic structure, whereas they have eight O and 12 Hf/Zr neighboring atoms in the tetragonal structure. In each sample, the lengths of the Hf-O and Hf-Hf/Zr bonds were similar to those of the Zr-O and Zr-Hf/Zr bonds, respectively, indicating that the local environments of the Hf and Zr atoms are similar to each other. The almost identical Hf and Zr coordination might benefit the homogeneous

TABLE II. EXAFS fitting results for monoclinic $Hf_{0.7}Zr_{0.3}O_2$ and tetragonal $Hf_{0.3}Zr_{0.7}O_2$. N is the assumed number of bonds, $R+\Delta$ is the scattering-phase-corrected interatomic distance, and σ^2 is the Debye-Waller factor.

	m-$Hf_{0.7}Zr_{0.3}O_2$			t-$Hf_{0.3}Zr_{0.7}O_2$		
Shell	N	$R+\Delta$ (Å)	σ^2 (Å^2)	N	$R+\Delta$ (Å)	σ^2 (Å^2)
Hf-O	7	2.17 ± 0.01	0.009 ± 0.001	4	2.11 ± 0.01	0.003 ± 0.001
				4	2.38 ± 0.02	0.006 ± 0.002
Zr-O	7	2.15 ± 0.01	0.007 ± 0.001	4	2.13 ± 0.01	0.003 ± 0.001
				4	2.40 ± 0.02	0.009 ± 0.003
Hf-Hf/Zr Zr-Hf/Zr	11	3.44–3.60	~0.02	12	3.53–3.69	~0.01

atomic scale mixing of the Hf-O and Zr-O clusters during the PEALD process. The synchronized coordination changes in the Hf-O and Zr-O clusters indicate the martensitic transition throughout the samples, as discussed in Sec. III B 1. The interatomic distances of the second shells (Hf-Hf/Zr or Zr-Hf/Zr) have broader ranges than those of the first shells (Hf-O or Zr-O) because the amount of the phase correction varies according to the abundance of atomic species in the neighborhood.

The second shell features [Hf(Zr)-Zr/Hf] were reduced significantly at $x\leq0.5$, as shown in Figs. 3(a) and 3(b). This suggests that the structural disorder in the networks between the Hf (or Zr)-O clusters are enhanced for $x\leq0.5$. The second shell σ^2 in the $x=0.3$ ($x=0.7$) sample was approximately 0.02 Å^2 (0.01 Å^2), which corresponds to a standard deviation of 0.14 Å (0.1 Å) in the bond lengths along the lateral bonding direction (see Table II). The enhanced disorder in the monoclinic samples ($x\leq0.5$) can be interpreted as a signature of the structural reconstruction in the networks of the Hf (or Zr)-O clusters. Compared to the tetragonal local structure, the monoclinic local structure has lower point-group symmetry[18] so that it can possess a larger number of configurations in the networks of the Hf(Zr)-O clusters. This can induce relatively higher diversity in the atomic configuration, resulting in enhanced structural disorder. However, the first-shell coordination in the HfZrO did not benefit the structural reconstruction because they are strongly bound with ionic bonding.[34] This can be confirmed by roughly similar first-shell peak intensities and σ^2 in Fig. 3 and Table II, respectively. For prefect HfO_2, the second shell features are significant due to the survival of long-range structural order.

C. Conduction bands

The change in the local structure results in a change in the electronic structure. The CB of the $Hf_{1-x}Zr_xO_2$ consists of metal d states (Hf 5d and Zr 4d states) at the lower energy range (<10 eV above the Fermi energy) and metal sp continuum states at the higher energy range. The O K-edge XAS reflects the density of states (DOS) of these CB states convoluted with the hybridization strength.[36,37] Figure 4(a) shows the O K-edge XAS spectra of the $Hf_{1-x}Zr_xO_2$ films. The metal d states were well separated in energy from the metal sp states, as shown by the vertical dashed line. The evolution in the overall line shape with increasing x was clearly observed. In particular, the unoccupied electronic structures of the Hf 5d and Zr 4d states varied considerably depending on x. Generally, the partial DOS of central metal ions are determined mainly by the local crystal field (CF) exerted by the surrounding oxygen orbitals.[38] Therefore, the coordination change due to a m-t structural transition will affect the electronic structure, as shown in Fig. 4(a). Figure 5 shows the (a) crystal structure and (b) resulting d state energy splitting in m-$Hf_{1-x}Zr_xO_2$ and t-$Hf_{1-x}Zr_xO_2$ films. The complex energy splitting can be interpreted by decomposing the coordination in the Hf/Zr-O clusters. Hf/Zr-O tetrahedral coordination with T_d site symmetry [shown in Fig. 5(a)] results in energy splitting into an e doublet and a t_2 triplet states,[38,39] as shown in Fig. 5(b). The eightfold Hf/Zr-O clusters in the tetragonal $Hf_{1-x}Zr_xO_2$, which have D_{2d} point-group symmetry, can be decomposed into two tetrahedra

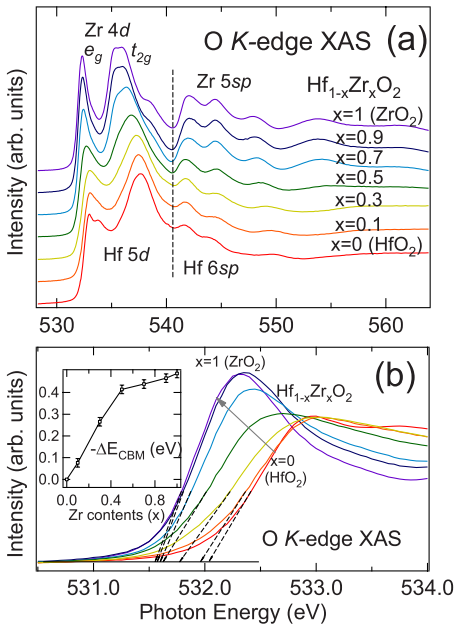

FIG. 4. (Color online) (a) O K-edge XAS spectra of the $Hf_{1-x}Zr_xO_2$ films and (b) their magnified view. The relative conduction-band edge energies $[-\Delta E_{CBM}=E_{CBM}(HfO_2)-E_{CBM}]$ from that of HfO_2, are plotted in the inset of (b) and tabulated in Table III.

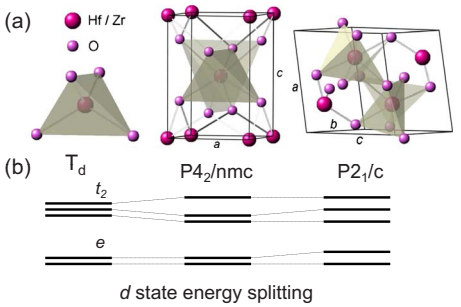

FIG. 5. (Color online) (a) Crystal structure and (b) the resulting d state energy splitting in m-$Hf_{1-x}Zr_xO_2$ and t-$Hf_{1-x}Zr_xO_2$ films. A Hf/Zr-O tetrahedral cluster (T_d symmetry) and corresponding d energy splitting into the e and t_2 states are appended.

(one of which is the space inversion of the other). Hence, the CF splitting should be similar to that of a single tetrahedron, except for the subscript "g" due to the inversion symmetry. The t_{2g} states were further split into a doublet and singlet, due to tetragonal elongation. However, the sevenfold Hf/Zr-O clusters in the monoclinic $Hf_{1-x}Zr_xO_2$, which have the C_1 symmetry, cannot be decomposed into two tetrahedrons. The lower site symmetry in the distorted clusters split all the states further, resulting in a sparse energy distribution, as shown in Figs. 4(a) and 5(b).

The minimum energy of the O K-edge XAS features changed according to the Zr content. Figure 4(b) shows the magnified view near the energy minima. The minimum energies were measured by extrapolating the lowest CB features at the steepest slopes in Fig. 4(b). They tend to decrease with increasing x. Generally the photon energy of the features in the O K-edge XAS spectra could vary depending on the chemical valences of the photon-absorbing oxygen atom because the energy cost for creating the core hole depends on the relaxation of the surrounding electrons. However, the decrease in the minimum energy with increasing x in Fig. 4(b) cannot be due to the chemical shift because the chemical shift would have also altered the binding energies (BEs) of the O 1s XPS spectra (see Fig. 7). The absence of a core hole effect indicates that the decrease truly reflects the change in the CB minimum (E_{CBM}) energy due to the smaller E_{CBM} of ZrO_2 than that of HfO_2.[14] The relative E_{CBM} with respect to HfO_2 (ΔE_{CBM}) are plotted in the inset and tabulated in Table III. The E_{CBM} decreased abruptly for $x \leq 0.5$, whereas it was almost saturated for $x \geq 0.7$. The linearity with x until $x \leq 0.5$ can be understood easily by considering the increase in the Zr 4d state below the CB edge of HfO_2 concurrently with the Zr content. This tendency will not be sustained and the E_{CBM} will be saturated when the DOS of Zr-related CB states becomes sufficiently large (*ad hoc* $x \geq 0.7$).

D. Valence bands and core-level XPS spectra

Figure 6 shows the valence-band (VB) spectra of the $Hf_{1-x}Zr_xO_2$ films. In contrast to the abrupt change in the CB structures, the VB structures barely changed with increasing Zr content. This is because the VB consists of relatively dispersed O 2p state whereas the CB is the localized Hf/Zr d states so that the VB features are rather insensitive to local coordination (as in Fig. 5) in contrast to the CB features. This suggests that the valence-electron configurations are relatively constant upon a compositional change. The BEs of the VB edges were approximately 3.2 eV at all the compositions. Combined with the decrease in E_{CBM} [in Table III and in the inset of Fig. 4(b)], this suggests that the band gap decreased by up to ~0.5 eV and that the reduction is due to the d band lowering with increasing x.

TABLE III. Relative CB minimum energies (E_{CBM}) of $Hf_{1-x}Zr_xO_2$ from that of HfO_2 defined as $\Delta E_{CBM} = E_{CBM} - E_{CBM}(HfO_2)$. The E_{CBM}s were measured by extrapolating the lowest CB features at the steepest slopes in Fig. 4(b). The values are plotted in the inset of Fig. 4(b).

Composition	ΔE_{CBM} (eV)
ZrO_2	−0.49
$Hf_{0.1}Zr_{0.9}O_2$	−0.47
$Hf_{0.3}Zr_{0.7}O_2$	−0.44
$Hf_{0.5}Zr_{0.5}O_2$	−0.41
$Hf_{0.7}Zr_{0.3}O_2$	−0.27
$Hf_{0.9}Zr_{0.1}O_2$	−0.08
HfO_2	0

The identical chemistry under the compositional change was also confirmed by the core-level XPS spectra in Fig. 7. The intensities of the (a) Hf 4f, (b) Zr 3d, and (c) O 1s main peaks changed according to their relative concentrations. Apart from the core-level spin-orbit splitting into doublets Hf($4f_{7/2}$,$4f_{5/2}$) and Zr($3d_{5/2}$,$3d_{3/2}$), each of the peaks had a simple Voigt line shape suggesting that the chemical balance in each atomic species is essentially invariant throughout the composition. It should be noted that the results of XAFS analyses evidenced that the local coordination of both Hf and Zr atoms changed from m- to t-local structures (in Sec. III B), even though the chemistry of all atoms appears to be invariant. The BEs of the Hf $4f_{7/2}$, Zr $3d_{5/2}$, and O 1s XPS main peaks were maintained at 17.1 eV, 182.6 eV, and 530.6 eV, respectively, indicating the 4+ valence of the Hf and Zr

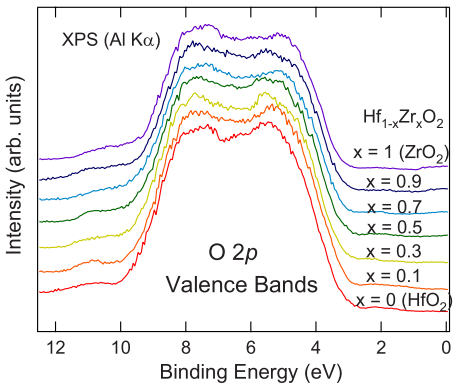

FIG. 6. (Color online) VB XPS spectra of the $Hf_{1-x}Zr_xO_2$ films taken with a monochromatic Al $K\alpha$ source. The similarity in the overall features and in the BEs of the VB maxima suggests a negligible change in the chemical balance.

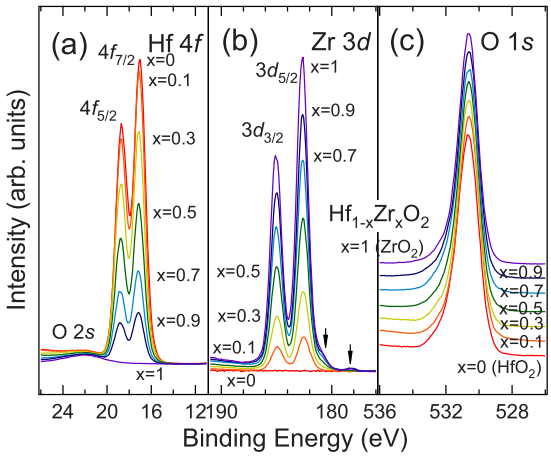

FIG. 7. (Color online) (a) Hf 4*f*, (b) Zr 3*d*, and (c) O 1*s* XPS spectra of the $Hf_{1-x}Zr_xO_2$ films taken with a monochromatic Al $K\alpha$ source. The BEs were similar regardless of the Zr content suggesting a similarity in chemical states even under the *m-t* local structural transition. The small right-side shoulders indicated by the arrows in (b) reflect Zr-silicide formation at the Si interface.

ions and high ionicity of the O ion.[15] Therefore, the *m-t* martensitic transition with increasing x was not accompanied by a significant change in the chemical balance between Hf, Zr, and O ions. The small right-side shoulders in the Zr 3*d* spectra [indicated by arrows in Fig. 7(b)] might reflect metallic Zr-silicide formation at the Si interface. However, this did not affect the structural and/or electronic properties of the films because the BEs of the Zr 3*d* main peaks did not change. Therefore, the structural transition occurred with negligible changes in the occupied electronic structure. This might benefit the uniform conversion of Hf/Zr-O local coordination from sevenfold to eightfold. The chemical invariance suggests that energy cost for the structural transition could be minimal so that it might be a necessary condition for the martensitic transition in the HfZrO system; further theoretical studies are required to clarify this issue.

IV. CONCLUSION

In conclusion, the martensitic transition from monoclinic to tetragonal structures with increasing Zr content (x) in $Hf_{1-x}Zr_xO_2$ composite oxides was accompanied by atomic-scale reconstruction. The local structures of both Hf and Zr atoms changed concurrently with the crystal structure. In the monoclinic oxides ($x \leq 0.5$), the networks between the Hf/Zr-O clusters showed enhanced bond disorder, indicating the complexity in the low-symmetry configuration. In addition, the evolution in the CB electronic structures with the structural changes was analyzed using cluster model approach. The x dependence of the CB energies was also discussed. The VB electronic structure and valence of each atomic species were relatively constant regardless of the compositional changes due to a negligible change in chemistry during the *t-m* martensitic transition.

ACKNOWLEDGMENTS

The authors acknowledge the supports from Hynix Co. through the system IC 2010 project of the Korean Government, and from National Research Foundation (NRF) funded by the Ministry of Education, Science and Technology (MEST) through the Converging Research Center Program (Grant No. 2009-0081961) and World Class University program (Grant No. R31-2008-000-10075-0). The authors thank Byeong-Gyu Park for help in the synchrotron experiments in PLS. The experiments at the PLS were supported in part by MEST and POSTECH.

*zax@snu.ac.kr
†cheolsh@snu.ac.kr

[1] http://www.intel.com/technology
[2] C. Hobbs, L. Fonseca, V. Dhandapani, S. Samavedam, B. Taylor, J. Grant, L. Dip, D. Triyoso, R. Hegde, D. Gilmer, R. Garcia, D. Roan, L. Lovejoy, R. Rai, L. Hebert, H. Tseng, B. White, and P. Tobin, Tech. Dig. VLSI Symp. **2003**, 9.
[3] H.-S. Jung, J.-H. Lee, S. K. Han, Y.-S. Kim, H. J. Lim, M. J. Kim, S. J. Doh, M. Y. Yu, N.-I. Lee, H.-L. Lee, T.-S. Jeon, H.-J. Cho, S. B. Kang, S. Y. Kim, I. S. Park, D. Kim, H. S. Baik, and Y. S. Chung, Tech. Dig. VLSI Symp. **2005**, 232.
[4] A. Kerber, E. Cartier, L. Pantisano, M. Rosmeulen, R. Degraeve, T. Kauerauf, G. Groeseneken, H. E. Maes, and U. Schwalke, IEEE Int. Reliab. Phys. Symp. Proc. **2003**, 41.
[5] G. Ribes, J. Mitard, M. Denais, S. Bruyere, F. Monsieur, C. Parthasarathy, E. Vincent, and G. Ghibaudo, IEEE Trans. Device Mater. Reliab. **5**, 5 (2005).
[6] M. Cho, J. H. Kim, C. S. Hwang, H.-S. Ahn, S. Han, and J. Y. Won, Appl. Phys. Lett. **90**, 182907 (2007).
[7] J. Park, M. Cho, H. B. Park, T. J. Park, S. W. Lee, S. H. Hong, D. S. Jeong, C. Lee, J. Choi, and C. S. Hwang, Appl. Phys. Lett. **85**, 5965 (2004).
[8] B. J. O'Sullivan, V. S. Kaushik, J.-L. Everaert, L. Trojman, L.-Å. Ragnarsson, L. Pantisano, E. Rohr, S. DeGendt, and M. Heyns, IEEE Trans. Electron Devices **54**, 1771 (2007).
[9] R. I. Hegde, D. H. Triyoso, S. B. Samavedam, and B. E. White, Jr., J. Appl. Phys. **101**, 074113 (2007).
[10] R. R. Manory, T. Mori, I. Shimizu, S. Miyake, and G. Kimmel, J. Vac. Sci. Technol. A **20**, 549 (2002).
[11] I. P. Studenyak, M. Kranjčec, O. T. Nahusko, and O. M. Borets, Thin Solid Films **476**, 137 (2005).
[12] D. H. Triyoso, R. I. Hegde, J. K. Schaeffer, R. Gregory, X.-D. Wang, M. Canonico, D. Roan, E. A. Hebert, K. Kim, J. Jiang, R. Rai, V. Kaushik, S. B. Samavedam, and N. Rochat, J. Vac. Sci. Technol. B **25**, 845 (2007).
[13] P. W. Peacock and J. Robertson, Phys. Rev. Lett. **92**, 057601 (2004).
[14] V. Fiorentini and G. Gulleri, Phys. Rev. Lett. **89**, 266101 (2002).
[15] D.-Y. Cho, S.-J. Oh, Y. J. Chang, T. W. Noh, R. Jung, and J.-C. Lee, Appl. Phys. Lett. **88**, 193502 (2006).
[16] E. Cockayne, Phys. Rev. B **75**, 094103 (2007).
[17] J. X. Zheng, G. Ceder, T. Maxisch, W. K. Chim, and W. K. Choi,

Phys. Rev. B **75**, 104112 (2007).
[18] D.-Y. Cho, J.-M. Lee, S.-J. Oh, H. Jang, J.-Y. Kim, J.-H. Park, and A. Tanaka, Phys. Rev. B **76**, 165411 (2007).
[19] G. D. Wilk, R. M. Wallace, and J. M. Anthony, J. Appl. Phys. **87**, 484 (2000).
[20] G.-M. Rignanese, F. Detraux, X. Gonze, A. Bongiorno, and A. Pasquarello, Phys. Rev. Lett. **89**, 117601 (2002).
[21] D. M. Adams, S. Leonard, D. R. Russell, and R. J. Cernik, J. Phys. Chem. Solids **52**, 1181 (1991).
[22] J. Kang, E.-C. Lee, and K. J. Chang, Phys. Rev. B **68**, 054106 (2003).
[23] P. Aldebert and J.-P. Traverse, J. Am. Ceram. Soc. **68**, 34 (1985).
[24] The reason why the ZrO_2 thin films or nanostructures favor a metastable tetragonal structure rather than the monoclinic structure, which has lower symmetry, has already been exploited extensively. The competition between the surface and bulk free energies should be primarily responsible for stabilizing the tetragonal phase, and the stress effect, nucleation, accessibility of external ions should be also considered. For a good review, see P. Southon, Ph. D. dissertation, University of Technology, 2000, and references therein.
[25] G. Lucovsky and G. B. Rayner, Jr., Appl. Phys. Lett. **77**, 2912 (2000).
[26] *X-Ray Absorption*, edited by D. C. Koningsberger and R. Prins (Wiley, New York, 1988).
[27] A. L. Ankudinov, B. Ravel, J. J. Rehr, and S. D. Conradson, Phys. Rev. B **58**, 7565 (1998).
[28] X. Zhao and D. Vanderbilt, Phys. Rev. B **65**, 233106 (2002).
[29] M. Winterer, R. Delaplane, and R. McGreevy, J. Appl. Crystallogr. **35**, 434 (2002).
[30] A. G. Khachaturyan, *Theory of Structural Transformations in Solids* (Wiley, New York, 1983).
[31] D. A. G. Bruggeman, Ann. Phys. **416**, 636 (1935).
[32] D. Stroud, Phys. Rev. B **12**, 3368 (1975).
[33] D.-Y. Cho, C.-H. Min, J. Kim, S.-J. Oh, and M. G. Kim, Appl. Phys. Lett. **89**, 253510 (2006).
[34] D.-Y. Cho, T. J. Park, K. D. Na, J. H. Kim, and C. S. Hwang, Phys. Rev. B **78**, 132102 (2008).
[35] M. A. Sahiner, J. C. Woicik, P. Gao, P. Mckeown, M. C. Croft, M. Gartman, and B. Benapfla, Thin Solid Films **515**, 6548 (2007).
[36] D.-Y. Cho, J. H. Kim, K. D. Na, J. Song, C. S. Hwang, B.-G. Park, J.-Y. Kim, C.-H. Min, and S.-J. Oh, Appl. Phys. Lett. **95**, 261903 (2009).
[37] D.-Y. Cho, J.-Y. Kim, B.-G. Park, K.-J. Rho, J.-H. Park, H.-J. Noh, B.-J. Kim, S.-J. Oh, H.-M. Park, J.-S. Ahn, H. Ishibashi, S.-W. Cheong, J.-H. Lee, P. Murugavel, T. W. Noh, A. Tanaka, and T. Jo, Phys. Rev. Lett. **98**, 217601 (2007).
[38] S. Sugano, Y. Tanabe, and H. Kamimura, *Multiplets of Transition-Metal Ions in Crystals* (Academic, New York, 1970).
[39] B. E. Douglas and C. A. Hollingsworth, *Symmetry in Bonding and Spectra* (Academic, New York, 1985).